WORLD CONFERENCE ON TIMBER ENGINEERING 2025
BRISBANE, AUSTRALIA

Advancing Timber for the Future Built Environment

NUMERICAL MODELLING OF ROCKING CLT SHEARWALL CONSIDERING THE WALL-TO-FLOOR INTERACTIONS

Chaoyue Zhang[1], Yuxin Pan[2]

ABSTRACT: The rocking behavior of cross-laminated timber (CLT) shearwalls is the primary kinematic motion that enhances energy dissipation in platform-type CLT building systems. During rocking, the vertical wall system inevitably interacts with horizontal floor system. At large lateral displacement, localized damage due to crushed fibers can occur to the rocking toe of wall and the face of floor This interaction affects the forces transferred to the connectors and subsequently influences the kinematic motion of the shearwall. However, many studies on the CLT shearwalls overlook the wall-to-floor interactions, either by treating shearwall as independent component of the seismic force resisting system or by employing a rigid diaphragm assumption. To achieve a realistic simulation of the rocking CLT shearwall, this paper first develops a beam-spring model that incorporates the nonlinear characteristics of connectors. The single- and coupled-panel wall models are validated against experimental results. To examine effects of different numerical representations of the wall-to-floor interactions, the beam-spring shearwall is integrated into a 3D model of a two-story conceptually designed coupled CLT shearwall system. Modal analysis has confirmed a reduced fundamental period of the shearwall system when adopting the rigid diaphragm. Furthermore, nonlinear dynamic analysis reveals significant differences in global lateral displacement and resistance, which can be attributed to the varying deformation demands, energy dissipation, and failure hierarchy of connectors.

KEYWORDS: Wall-to-floor interactions, rocking CLT shearwall, nonlinear analyses, OpenSees modelling.

1 – INTRODUCTION

1.1 PLATFORM-TYPE CLT SHEARWALL

Seismic force resisting systems (SFRSs) characterized by cross-laminated timber (CLT) shearwalls have now been included in many building codes. NBCC 2020 [1] introduces a ductility-related seismic force modification factor, R_d=2, and an overstrength-related factor, R_o=1.5, for moderately ductile platform-type CLT shearwalls. ASCE 7-22 [2] also specifies response modification factor, R=3, for CLT shearwalls. The lateral resistance and inelastic deformability of such SFRS primarily count on the in-plane stiffness of CLT panels and the ductility of mechanical connectors, such as hold-downs (HDs), shear brackets (SBs), and vertical joints (VJs).

In platform-type CLT buildings, the metal connectors integrate the vertical wall system and the horizontal floor system as an integral SFRS. To resist overturning and horizontal shear forces, designated connectors are designed to facilitate the preferrable rocking wall behavior and dissipate earthquake energy. Many studies focus on introducing new yielding dampers and self-centering devices to enhance ductility and reduce drift of CLT shearwall [3]–[5]. However, these studies often treat the wall member as an isolated part of the SFRS and often ignore the wall-to-floor interactions.

1.2 WALL-TO-FLOOR INTERACTIONS

As the overturning force increases, shearwalls inevitably interact with floor slabs through the gap opening at the uplifted end as well as the vertical settlement at the compressed rocking toe. When shear wall rocks at large displacement, localized crushing and splitting of wood fibers can occur to those severely stressed areas at both wall ends and slab faces. Amer et al. [6] tested and quantified the progressive damage states of CLT shearwall, from fine splits to excessive end rolling. In a multistory CLT building, floors serve as the foundation for the shearwalls above. Conceivably, the vertical stiffness of foundation would affect lateral response of shearwall. Wichman et al. [7] performed shake table test on a two-story rocking CLT shearwall and found that the unexpected vertical flexibility of foundation has significant effects on structure system's dynamic response: it exhibited longer fundamental period due to reduced stiffness and smaller story drift when

[1] Chaoyue Zhang, PhD Student, Sustainable Timber and Structural Safety Lab, Department of Civil and Environmental Engineering, The Hong Kong University of Science and Technology, Hong Kong, China, czhangdu@connect.ust.hk

[2] Yuxin Pan, Assistant Professor, Sustainable Timber and Structural Safety Lab, Department of Civil and Environmental Engineering, The Hong Kong University of Science and Technology, Hong Kong, China, ceypan@ust.hk

https://doi.org/10.52202/080513-0401

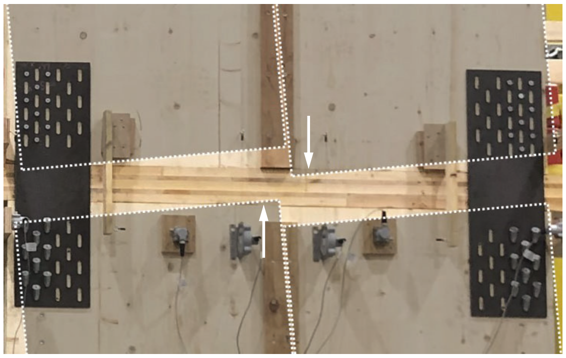

Figure 1. Wall-floor rocking interface.

comparing to a model with idealized rigid foundation. Fischer and Schafer [5] indicated that the in-plane flexibility of floor slabs also affects building's fundamental period and can dominate the global seismic response when vertical members are stiff.

Additionally, the downward and upward settlement caused by the bottom corner of the upper story wall and the top corner of the lower story wall will exert counteracting vertical forces on the floor slab, as illustrated in Fig. 1. The force pair can lead to obvious flexural and shear deformation across the depth of CLT panel. Such deformation was well captured during the cyclic test on a two-story CLT house performed by Popovski and Gavric [8]. Moreover, to quantify contribution of the out-of-plane bending stiffness of CLT floor to global rocking stiffness, D'Arenzo et al. [9] leveraged the Wrinkler Model to represent the wall-to-floor interface and revealed the modified kinematic motions of single and coupled CLT shearwalls due to the out-of-plane action of CLT floor.

At building system level, depending on the layout of floor plan, the wall-to-floor interactions may cause unintentional coupling of CLT shearwalls aligned along the loading direction and those aligned orthogonally. In this case, the inclusion of actual mechanical properties of CLT floor would play a pivotal role in affecting the vertical and horizontal forces transferred between floor and wall, the in-plane and out-of-plane actions of shearwall, as well as deformation demands placed on connectors. In wall-frame structural system, similar unintentional coupling effect can occur to the SFRS and the gravity system due to a global 3D outrigger action related to the wall-to-floor interactions, which ultimately results in excessive axial forces on reinforced concrete columns [10]. In building systems composed of CLT shearwall and timber frame, such interactions might impose significant moment demands on the beam-to-column joints, which may not be preliminarily designed to sustain large rotational demands.

Despite those critical effects of wall-to-floor interactions, systematic instrumentation at those highly stressed regions of CLT panels is very limited and so is the quantitative assessment of the actual deformation of CLT shearwall and floor. For CLT shearwall building systems, the global impacts of such interactions are also rarely studied.

1.3 DESIGN OF CLT SHEARWALL

Most seismic design codes assume rigid floor diaphragm and treat shearwall as an isolated part of a SFRS. Alternatively, if the vertical wall is deemed rigid, ASCE 7-22 (12.10.4) allows yielding of diaphragm and proposes response modification coefficient, R_s, mainly to account for its in-plane stiffness. For multistory CLT building, its floor diaphragm should not be simply idealized as rigid given those effects of wall-to-floor interactions pertaining to the actual in-plane and out-of-plane deformability of CLT floor. Meanwhile, the rocking CLT shearwall cannot be considered rigid since it is mainly responsible for dissipating major seismic energy. In those regards, the deficiency in code presumptions might results in unexpected global and local responses of multistory CLT shearwall buildings.

1.4 CONVENTIONAL MODEL

In terms of numerical modelling of CLT building, many studies adopt the rigid diaphragm constraint, disregarding any interactions involving deformability of floor slabs. Such constraint would create untrue boundary conditions, enforcing the sliding motion and hampering rocking motion of shearwall. Besides, the gap opening and the compression zone are often simplified as two springs situated at two ends of wall, as shown in Fig. 2. To enable rocking about a pivot point, many works simply assign each spring with the *elasticNoTension* material in OpenSees [11] and an arbitrarily large compressive stiffness, without accounting for the magnitude and profile of compressive stress distribution. Therefore, as the CLT building story goes higher, adopting the rigid diaphragm constraint and simplified representation of wall-to-floor interface would lead to increasingly inaccurate results. Beyond elastic range, different numerical representations of wall-to-floor interactions would affect deformation demands in connectors between walls and floors, which can change the failure hierarchy of connectors, modify the overstrength and ductility of SFRS, and subsequently determine the global collapse limit state of building system.

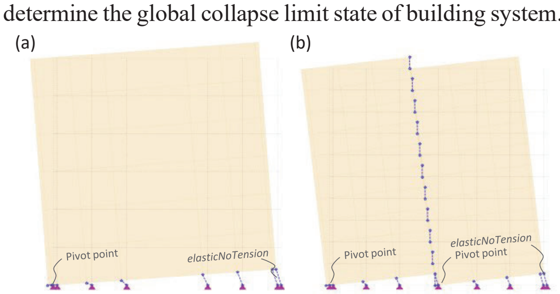

Figure 2. Conventional model (a) single panel and (b) coupled panel.

This research intends to develop numerical model for multistory platform CLT shearwall systems considering the wall-to-floor interactions. To reproduce realistic rocking behavior of CLT shearwall, this work proposes a beam-spring model that incorporates both nonlinearities of connector and compressive properties of CLT shearwall. Based on that, 3D models of a two-story floor coupled CLT shearwall are established to quantify differences in local and global responses due to different numerical representations of wall-to-floor interactions.

https://doi.org/10.52202/080513-0401

2 – MODELLING AND VALIDATION

2.1 THE BEAM-SPRING REPRESENTATION

Conventionally, the CLT shearwall is modelled by excessive shell elements (e.g., *ShellMITC4* elements in OpenSees) finely meshed according to spring's location, as shown in Fig. 2. To reduce model complexity and meanwhile to capture potential shear and flexural deformations, this work uses the *ElasticTimoshenkoBeam* elements to model the CLT shearwall. As depicted in Fig. 3, to connect the beam element and all spring elements, the lower end node of beam is deemed as the primary node (red square), where the *ndJ* nodes (black square) of all springs are connected via the *RigidLink* constraint.

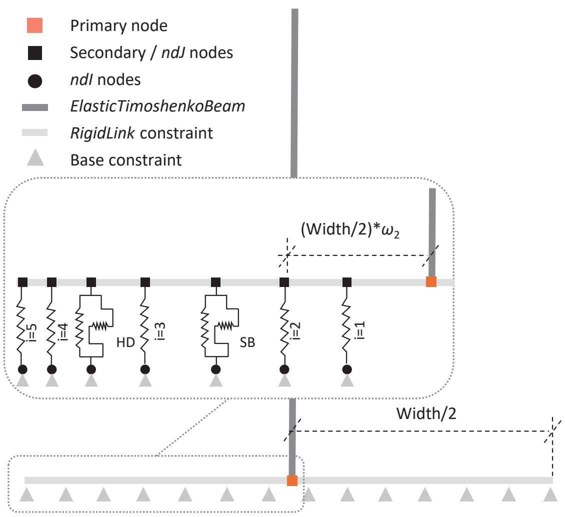

Figure 3. The beam-spring model.

To model the formation of compression zone of the rocking beam-column connection in precast concrete members, Spieth et al. [12] proposed using multiple springs distributed along the contact interface by following the *Lobatto* Integration scheme, which defines a denser number of contact points around the compression toe. Building on this method, this paper adopts a series of discrete contact springs and connector springs to represent the continuous wall-floor interface. Fig. 3 has zoomed in a total of 5 contact springs, plus 1 connector springs for HD, and 1 connector springs for SB. For both vertical and horizontal translational degree-of-freedom (DOF), nonlinearities of connector spring are embedded in the calibrated hysteretic materials assigned to *ZeroLength* element. For the contact springs, instead of using *elasticNoTension* material, this model uses *ElasticPPGap* material to account for compression stiffness and potential yielding of fibers. This is to best produce realistic reaction forces and compressive deformation when shearwall rocks. To obtain the vertical stiffness, K_i, for each contact spring, a total contact stiffness, K, can be determined by:

$$K = \frac{A \cdot E}{l_p};\ K_i = K \cdot \omega_i \qquad (1)$$

Where A and E are the cross-sectional area and elastic of moduli of the CLT panel; l_p is the estimated plastic hinge length suggested by [13]. Then the contact stiffness for individual spring, K_i, equates the weighted value of total K based on the weights, ω_i, of the Lobatto Integration. Similarly, location or abscissas of individual spring is determined by the weighted portion of half width of wall base. Yielding force of spring, F_y, can be calculated from the product of yielding strength of CLT under compression, f_c, and the weighted cross-sectional area, as in:

$$F_y = f_c \cdot A \cdot \omega_i \qquad (2)$$

2.2 ONE-STORY CLT SHEARWALL

To validate the beam-spring model, numerical models for both single and coupled CLT shearwalls are developed. Geometry of the models corresponds to the tested wall configuration I,2 and III,7, as presented in [14]. Nonlinear degradation properties of HD, SB, and VJ are calibrated according to the cyclic test results in [15]. Fig. 4 has presented the calibrated *HystereticSM* material for HD and VJ. A total of 10 discrete contact springs were used.

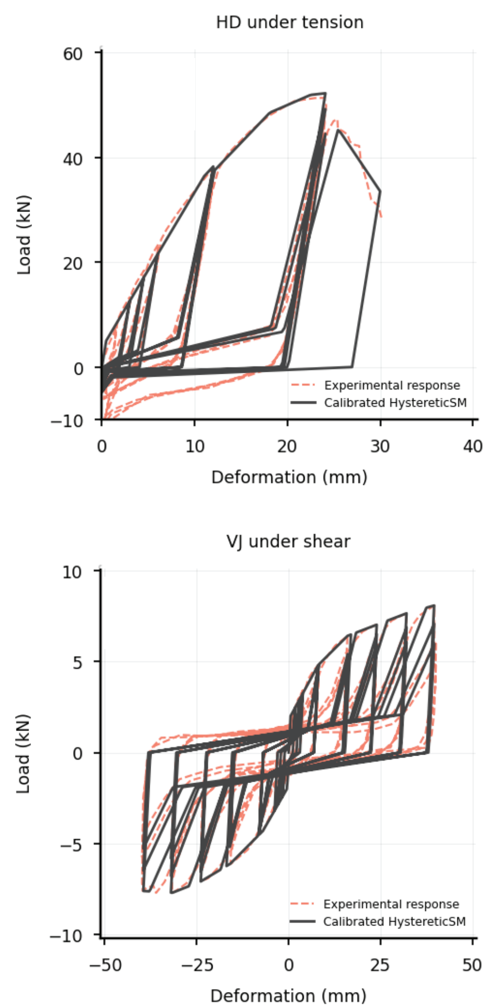

Figure 4. Calibrated material for HD and VJ.

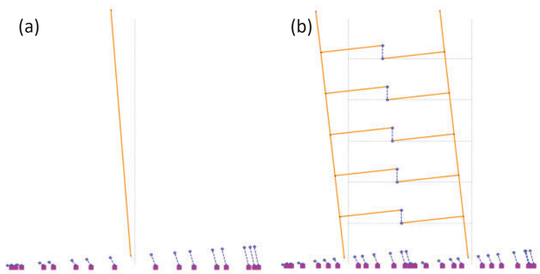

Figure 5. wall models (a) single panel and (b) coupled panel.

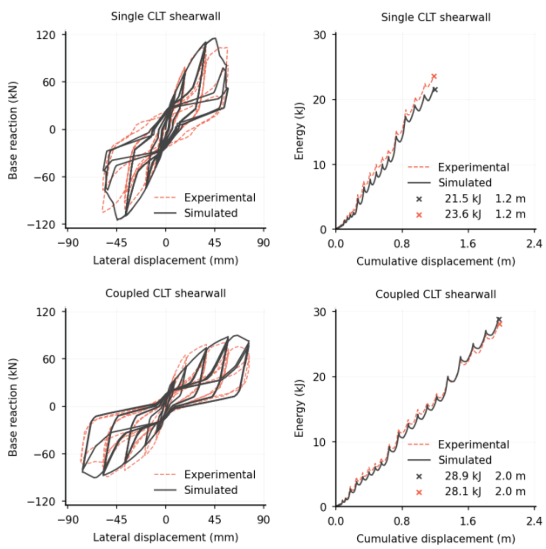

Figure 6. Cyclic curves and hysteretic energy.

Fig.5 shows the deformed shapes of CLT shearwalls. The rocking behavior of shearwall is associated with the rotation of beam element and the deformation of spring elements. Notice that the bottom part of wall rocks based on the idealization that the edge remains as a rigid plane. The strength and stiffness degradation patterns are reproduced by those hysteretic curves, as depicted in Fig. 6. However, for the single CLT shearwall, a more severe pinching effect is observed on the simulated response. This can be explained by the difference in the reloading stiffness between experimental test data and calibrated material response of HD and SB under tension. While for VJ under shear, adopting the *HystereticSM* model can achieve a more accurate calibration. Additionally, it is observed that the simulation results overestimate the peak capacity for single and coupled CLT shearwall. This potentially attribute to the variability in connector behavior exhibited in component test and shearwall test. Looking at the cumulative hysteretic energy, the beam-spring model can achieve satisfactory agreements with test result for both types of shearwall. Overall, single CLT shearwall manifests higher elastic stiffness and ultimate strength. Conversely, coupled CLT shearwall possesses higher ductility due to the contribution from the inelastic deformation of VJs. This also corresponds to the larger cumulative displacement and higher total energy dissipated from the coupled CLT shearwall.

3 – FLOOR COUPLED CLT SHEARWALL

3. 1 SHEARWALL CONFIGURATION

Masroor et al. [16] recently tested the lateral performance of a two-story CLT shearwall with the presence of CLT floor. To represent a more common form of multistory residential CLT buildings, where cross walls are coupled by the floors to resist lateral loads, this paper expanded the tested specimen to a floor coupled shearwall system. Two 3D models were developed in OpenSees to study effects of wall-to-floor interactions for such prototype. For Model I, the CLT floor is modelled by the *ShellMITC4* elements, as shown in Fig.7a. To consider equivalent in-plane and out-of-plane elastic properties of CLT, including elastic moduli, shear moduli, and Poisson's ratios, a *PlateFiber* section assigned with *ElasticOrthotropic* material is defined. A comparative 3D shearwall model, Model II (see Fig. 7b), featuring rigid diaphragm assumption is also developed to quantify differences in global response of building system and local response of various connectors. Notice that this work only uses two *ZeroLength* elements to represent the VJs. The envelop of VJ's cyclic behavior is linearly scaled based on the actual pairs of screws in half-lap joints [17].

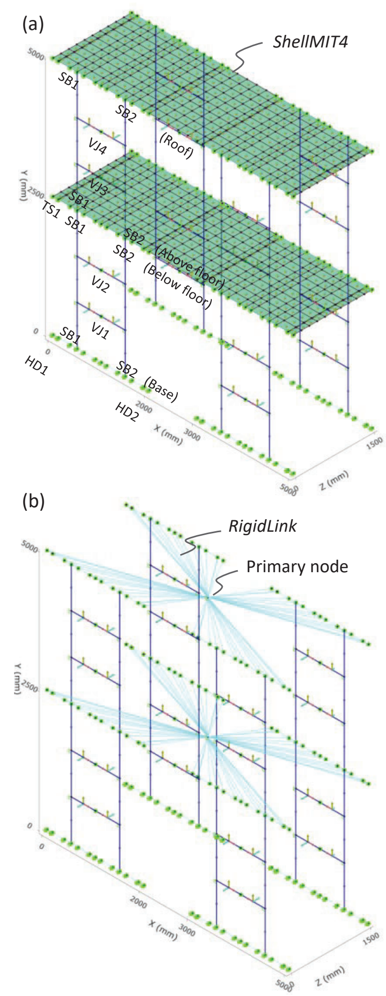

Figure 7. Floor coupled CLT shearwall (a) Model I and (b)Model II.

https://doi.org/10.52202/080513-0401

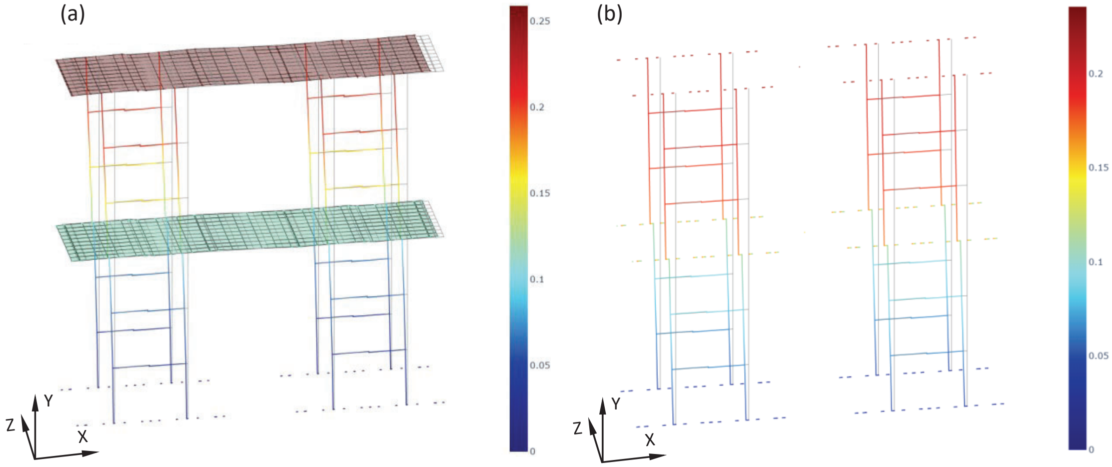

Figure 8. Mode shapes (a) Model I and (b) Model II.

3.2 MODAL PROPERTIES

For Model I, the applied dead load and the self-weight of CLT floor are converted to mass density, which is then assigned to the *ElasticOrthotropic* material. According to the test setup in [16], A dead load of 2 tons was applied to a floor plan measuring 2.0 m by 1.5 m at each story. Consequently, a total of 4 tons of dead load was applied at each story, considering the side-by-side shearwall layout. The density of CLT panel was taken as 475 kg/m^3. Additionally, the self-weight of CLT shearwall was converted to mass per length assigned to the *ElasticTimoshenkoBeam*. This approach aims to best represent the actual mass distribution of the structure system. For Model II with rigid diaphragm, the dead load and floor weight were lumped at the two primary nodes at floor and roof levels, respectively.

The fundamental translational mode shapes in the X direction of Model I and Model II are depicted in Fig. 8. The corresponding fundamental periods for the two models are 0.167 sec and 0.119 sec, respectively. The shorter period of Model II suggests a higher initial elastic stiffness, corresponding to the idealization that the wall-to-floor interactions are neglected, and the floor deformability is excluded. This is also associated with the higher modal participation ratio of 91.13% for translation in the X direction than that of 81.97% for Model II. Conversely, Model I's floor exhibits noticeable out-of-plane deformation, as shown in Fig. 8a, at the juncture where the rocking coupled CLT shearwall causes misalignment in the Y direction due to shear deformation of VJs. In addition, for the CLT floor segment coupling the shearwalls side-by-side, significant out-of-plane actions would also occur when the two aligned shearwalls rock together.

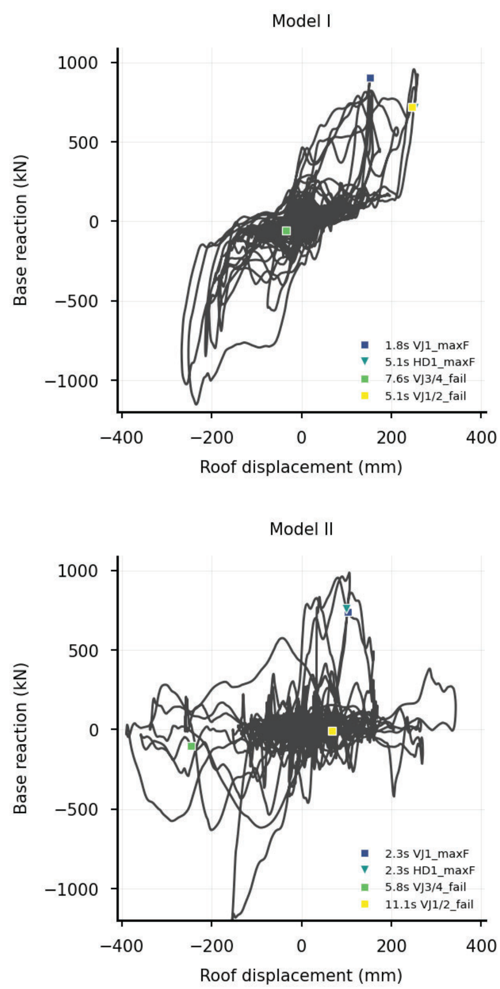

Figure 9. Base shear- roof displacement (a) Model I and (b) Model II.

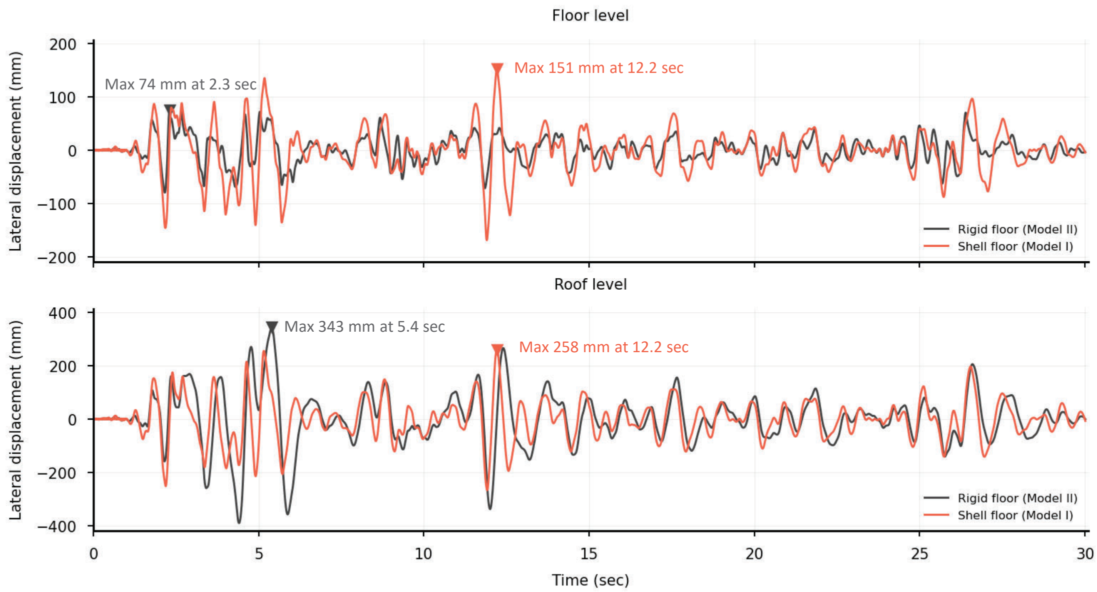

Figure 10. Time history of story displacement (a) Model I and (b) Model II.

3.3 DYNAMIC ANALYSIS

Global Response

To quantify effects of wall-to-floor interaction on the nonlinear dynamic behavior of the coupled CLT shearwall, Model I and II were subjected to the EI Centro ground motion record scaled to a high intensity (peak ground acceleration of 3g) considering the overdesigned test specimen in [16]. Fig. 9 illustrates the relationship between base shear and roof displacement. Both global hysteretic curves exhibit distinctive nonlinear patterns. Specifically, Model I's hysteretic curve shows the characteristic pinching behavior when the structure system oscillates at large displacement when ground motion reaches high amplitude pulses. Meanwhile, its lateral resistance maintained at a high level even when roof displacement exceeds 200 mm. Dissimilarly, Model II experiences a substantial loss of strength before roof displacement approaches 200 mm. Beyond this point, the simulation results indicate that the shearwall system can only provide a resistance about 500 kN, approximately 50% less than its maximum capacity.

The deformation states of selected connectors are also annotated on Fig. 9. In general, the timings of HD and VJ reaching the two limit states—the maximum and the failure points—differ, clearly indicating a varying time history of deformation. A detailed comparison of hysteretic response of connectors is presented in the next section.

Fig. 10 compares the time history of floor and roof displacement. At the floor level, Model I consistently exhibits larger displacements than Model II throughout the entire time history, particularly at high peaks. The maximum floor displacement of Model I has reached 151 mm, which is twice that of Model II. To the opposite, at the roof level, Model II shows larger displacement during the first 6 secs, with a peak displacement of 343 mm, 33% higher than that of Model I. Those differences in story displacement reflect that adopting the rigid floor constraint places higher demands at the roof level while the lower floor shows much smaller drift. Consequently, the deformation of connectors at two stories, including the uplift of HDs, the sliding of SBs, and the shearing of VJs, would exhibit different nonlinear behaviors and degradation patterns.

Local Response

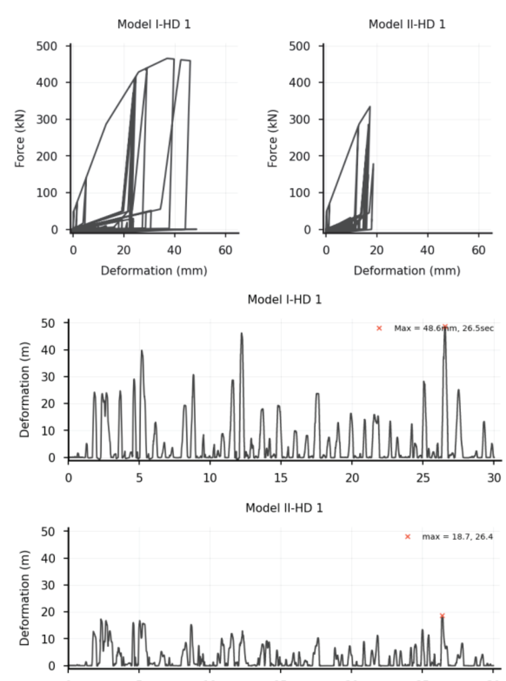

Figure 11. Comparison of HD response.

https://doi.org/10.52202/080513-0401

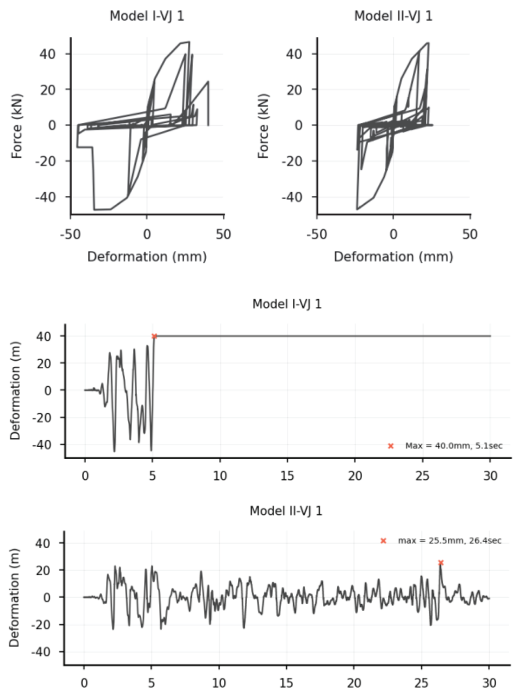

Figure 12. Comparison of VJ response.

Fig. 11 and Fig. 12 compare the hysteretic behavior and deformation history between Model I and Model II for HD and VJ, respectively. Notably, HD in Model I has experienced incredibly higher nonlinear behavior, as evidenced by the yielding, capping, and descending trends of the force-deformation envelop. The maximum deformation of HD in Model I reaches 48.6 mm, compared to 18.7 mm for HD in Model II. Regarding the VJ, the envelop of hysteretic curves of Model I shows a bulkier shape due to larger deformation demands. In addition, the maximum deformation of VJ in Model I has reached a predefined failure point at 40 mm. The deformation history clearly illustrates that this failure is caused by the high-amplitude oscillation of ground motion at the first 5 seconds. On the other hand, if adopting the rigid floor constraint, Model II's VJ would deform under a maximum value of 25.5 mm.

To quantify cumulative demands in resistance and deformation, Fig. 13 presents the total and the individual energy dissipated by every single connector. Overall, for Model I, energy dissipation due to inelastic deformation of all connectors has reached 566.7 kJ, which is 80% higher than that of Model II. This corresponds to Model II's substantial loss of global lateral resistance at large displacement, disabling the structure system from dissipating more energy. To be specific, HD and tension strap (TS) are responsible for dissipating the majority of earthquake energy. Model I' HD accounts for 44.8% while Model II's HD only accounts for 24.9%. In return, TSs (blue portion) and SBs (green portion) of Model II have dissipated more energy than those in Model I. Besides, it is observed that VJs in both models contribute minimally to energy dissipation, attributed to VJ's limited capacity.

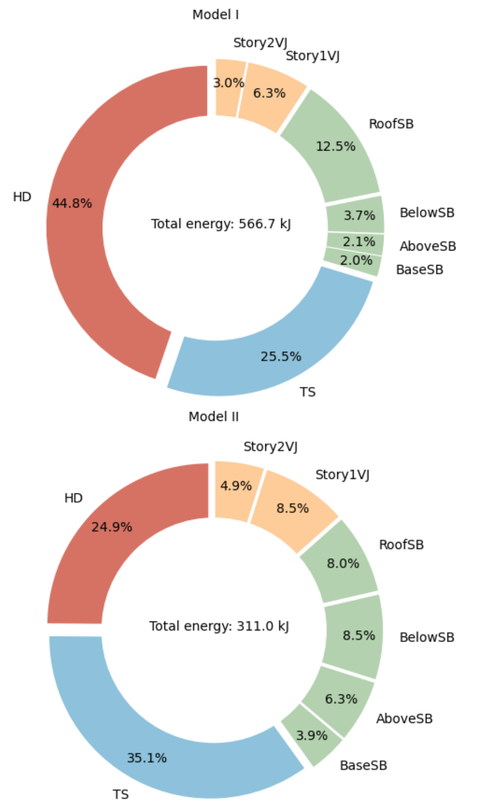

Figure 13. Comparison of energy dissipated by different connectors.

Based on the local responses of connectors, it can be concluded that adopting the rigid floor constraint, equivalently overlooking wall-to-floor interactions, shifts local deformation demands towards the SBs and TSs. Under such circumstances, the designated energy dissipator, namely the high-capacity HD at the base, would fail to facilitate the major rocking behavior of shearwall through HD's uplift. Instead, the excessive shifted deformation of SBs would cause more sliding of shearwall. Moreover, this leads to a different failure hierarchy of connectors, which can subsequently generate misleading simulation results and inaccurate performance assessments.

4 – CONCLUSION

This paper develops numerical models for the rocking CLT shearwall system taking into account the wall-to-floor interactions. Specifically, this work applies a validated beam-spring model to the CLT shearwall and integrates it to a 3D shearwall system model with two different numerical representations of floor. To quantify effects of wall-to-floor interaction on a two-story floor coupled CLT shearwall system, this paper compares the modal properties and nonlinear dynamic responses. It is confirmed that adopting the rigid diaphragm assumption in modeling CLT platform shearwall structure reduces the fundamental period of the system. Under earthquake excitation, the two models exhibited rather different lateral displacements at

https://doi.org/10.52202/080513-0401

two stories, primarily due to the varying deformation demands placed on HD, TS, VJ, and SB.

It should be noted that the presented work was based on numerical assessment of a conceptually designed floor coupled CLT shearwall system. Future work will focus on experimental tests to study how actual deformability of floor affects CLT shearwall behavior. Extensive numerical analyses will also be conducted to further examine the effects of wall-to-floor interactions on a code-compliant building system.

ACKNOWLEDGEMENT

This research was supported by the Research Grants Council of the Hong Kong Special Administrative Region, China (Project No. 26204623) and the National Natural Science Foundation of China (Grant No. 52308280).

REFERENCES

[1] NBCC, *National Building Code of Canada*, vol. 1. 2020.

[2] American Society of Civil Engineers, “ASCE 7-22 Minimum Design Loads and Associated Criteria for Buildings and Other Structures,” *Minim. Des. Loads Assoc. Criteria Build. Other Struct.*, Nov. 2021, doi: 10.1061/9780784415788.

[3] Y. Pan, C. Dickof, and T. Tannert, “Seismic performance evaluation of self-centering balloon-framed CLT building,” *Eng. Struct.*, vol. 294, no. June, p. 116821, 2023, doi: 10.1016/j.engstruct.2023.116821.

[4] N. Chan, A. Hashemi, S. Agarwal, P. Zarnani, and P. Quenneville, “Experimental Testing of a Rocking Cross-Laminated Timber Wall with Pinching-Free Connectors,” *J. Struct. Eng.*, vol. 149, no. 10, pp. 1–18, 2023, doi: 10.1061/jsendh.steng-12389.

[5] B. Moerman, M. Li, T. Smith, and H. Lim, “Design and cyclic testing of bolted end plate connections between steel link beams and cross-laminated timber for coupled shear walls,” *Constr. Build. Mater.*, vol. 353, no. August, p. 129060, 2022, doi: 10.1016/j.conbuildmat.2022.129060.

[6] A. Amer, R. Sause, and J. Ricles, “Experimental Response and Damage of SC-CLT Shear Walls under Multidirectional Cyclic Lateral Loading,” *J. Struct. Eng.*, vol. 150, no. 2, pp. 1–12, 2024, doi: 10.1061/jsendh.steng-12576.

[7] S. Wichman, J. W. Berman, and S. Pei, “Experimental investigation and numerical modeling of rocking cross laminated timber walls on a flexible foundation,” *Earthq. Eng. Struct. Dyn.*, vol. 51, no. 7, pp. 1697–1717, 2022, doi: 10.1002/eqe.3634.

[8] M. Popovski and I. Gavric, “Performance of a 2-Story CLT House Subjected to Lateral Loads,” *J. Struct. Eng.*, vol. 142, no. 4, pp. 1–12, 2016, doi: 10.1061/(asce)st.1943-541x.0001315.

[9] G. D’Arenzo, S. Schwendner, and W. Seim, “The effect of the floor-to-wall interaction on the rocking stiffness of segmented CLT shear-walls,” *Eng. Struct.*, vol. 249, no. September, 2021, doi: 10.1016/j.engstruct.2021.113219.

[10] R. E. Sedgh, R. P. Dhakal, C. L. Lee, and A. Carr, “System Overstrength Factor Induced By Interaction Between Structural Reinforced Concrete Walls, Floors and Gravity Frames-Analytical Formulation,” *Bull. New Zeal. Soc. Earthq. Eng.*, vol. 55, no. 3, pp. 138–154, 2022, doi: 10.5459/BNZSEE.55.3.138-154.

[11] OpenSees, “Open System for Earthquake Engineering Simulation - Home Page.” 2006, Accessed: Sep. 15, 2020. [Online]. Available: https://opensees.berkeley.edu/.

[12] H. A. Spieth, A. J. Carr, A. G. Murahidy, D. Arnolds, M. Davies, and J. B. Mander, “Modeling of post-tensioned precast reinforced concrete frame structures with rocking beam-column connections,” *New Zeal. Soc. Earthq. Eng. Conf. 2004*, no. 32, 2004, [Online]. Available: http://db.nzsee.org.nz/2004/Paper32.pdf.

[13] T. Akbas *et al.*, “Analytical and Experimental Lateral-Load Response of Self-Centering Posttensioned CLT Walls,” *J. Struct. Eng.*, vol. 143, no. 6, pp. 1–15, 2017, doi: 10.1061/(asce)st.1943-541x.0001733.

[14] I. Gavric, M. Fragiacomo, and A. Ceccotti, “Cyclic Behavior of CLT Wall Systems: Experimental Tests and Analytical Prediction Models,” *J. Struct. Eng.*, vol. 141, no. 11, pp. 1–14, 2015, doi: 10.1061/(asce)st.1943-541x.0001246.

[15] I. Gavric, M. Fragiacomo, and A. Ceccotti, “Cyclic behaviour of typical metal connectors for cross-laminated (CLT) structures,” *Mater. Struct. Constr.*, vol. 48, no. 6, pp. 1841–1857, 2015, doi: 10.1617/s11527-014-0278-7.

[16] M. Masroor, ; Mahtab Gheisari, T. Tannert, and M. Asce, “Experimental Parameter Study of Two-Story Platform-Type CLT Shear Walls,” *J. Struct. Eng.*, vol. 150, no. 8, Aug. 2024, doi: 10.1061/JSENDH.STENG-13277.

[17] Y. Pan, T. Teflissi, and T. Tannert, “Experimental Parameter Study on CLT Shear Walls with Self-Tapping Screw Connections,” *J. Struct. Eng.*, vol. 150, no. 1, pp. 1–13, 2024, doi: 10.1061/jsendh.steng-12710.

https://doi.org/10.52202/080513-0401